The spectrum of open confining strings in the large-N_c limit

Confinement and symmetry from vacuum to QCD phase diagram, 2025, Benasque Science Center

Pedro Bicudo [1], Alireza Sharifian [2], Andreas Athenodorou [3]

[1] CeFEMA and Physics department, Instituto Superior Técnico, Av. Rovisco Pais, 1049 Lisboa, Portugal;
[2] CeFEMA and Physics department, Instituto Superior Técnico, Av. Rovisco Pais, 1049 Lisboa, Portugal;
[3] Computation-based Science and Technology Research Center, The Cyprus Institute, Cyprus;

[1] *bicudo@tecnico.ulisboa.pt,* [2] *alireza.sharifian@tecnico.ulisboa.pt,* [3] *a.athenodorou@cyi.ac.cy*

February 10, 2025

Abstract

We compute the spectra of open flux tubes formed between a static quark-antiquark pair for various gauge groups in the large-N_c limit, focusing on different symmetries manifested by the quantum numbers of angular momentum, parity, and charge conjugation.

Specifically, we present spectra from $N_c = 3$ up to $N_c = 6$ and for eight different irreducible representations of the symmetry characterizing the flux tube. In this study, we employed an anisotropic Wilson action, a large number of suitable spacial operators, and solved the generalized eigenvalue problem (GEVP) to obtain a significant number of excitations for different combinations of flux tube quantum numbers.

The spectra are compared with the Nambu-Goto string model, revealing novel phenomena such as the presence of massive axions in the flux tube spectrum. We find that the mass of the axion in the open flux tube spectra sector is consistent with the mass obtained in the closed flux tube sector.

Preamble

- In QCD, heavy quarks are confined in bound states by flux tubes.
- Long flux tubes behave similarly to thin strings.
- Strings have are $D-2$ massless Goldstone modes from broken translation invariance in the $D-2$ directions.
- There should be a low energy Effective String Theory model describing the energy spectrum of the QCD flux tubes.
- How accurate is such an effective string theory as an approximation?
- Are there additional massive excitations along the flux tube?

Preamble

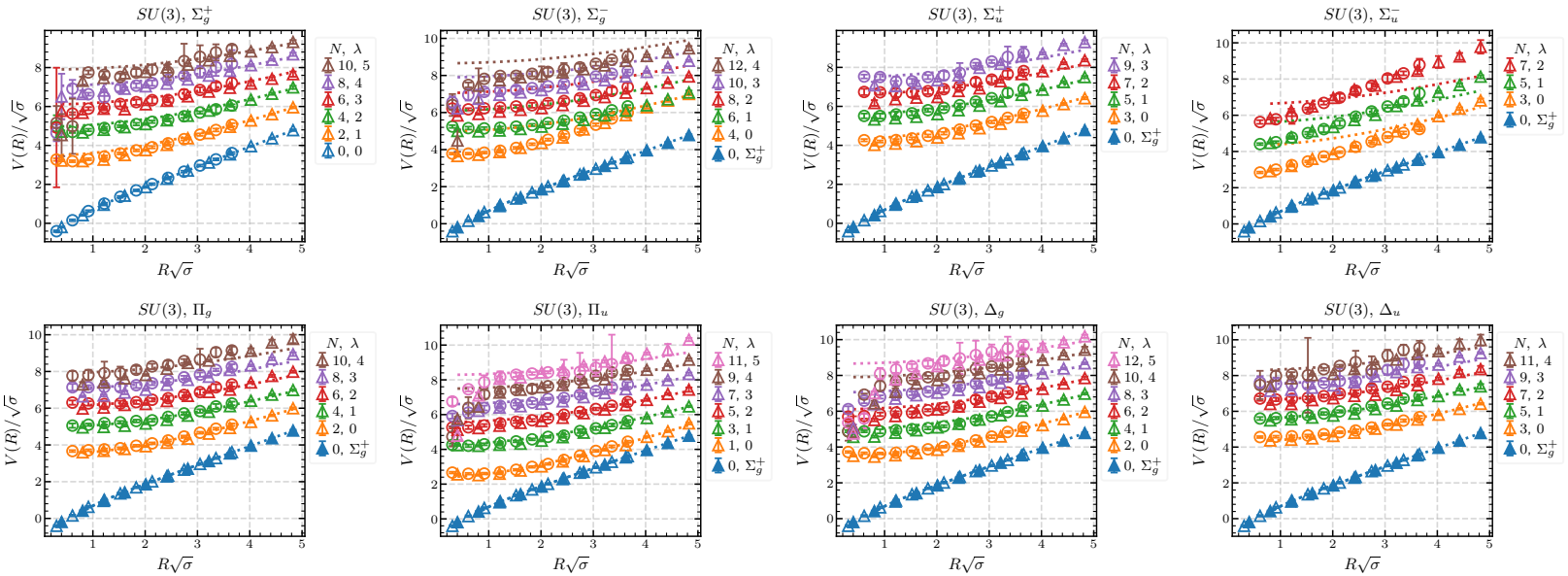

Figure 1: Eight SU(3) spectra [Sharifian *et al.*(2023)Sharifian, Cardoso, and Bicudo]. Polygonal shapes in each figure show the simulation with bare anisotropy $\xi = 4$, while circle markers indicate $\xi = 2$. N is the quantum number as defined in Eq. 2, and λ is the excitation number.

- In the open flux tube framework, the spectrum with negative-parity and angular momentum Σ suggest the presence of a worldsheet axion.

Preamble

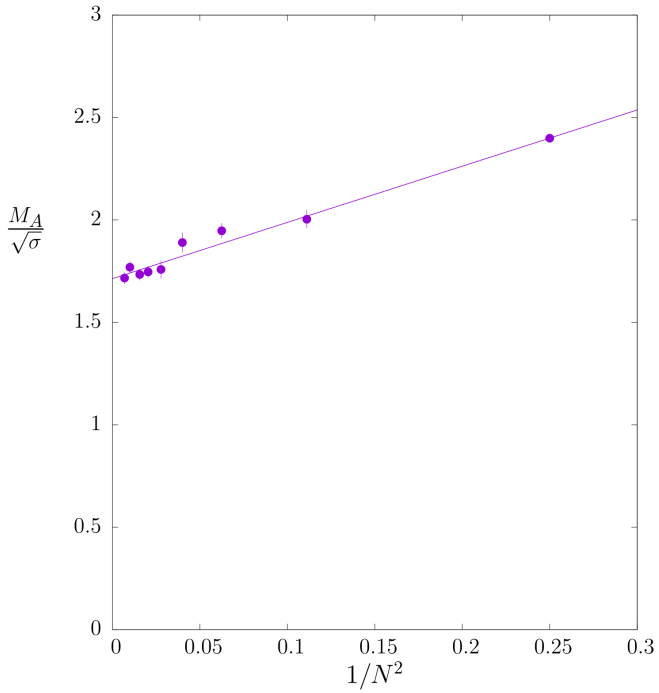

Figure 3: The 'axion' mass, using eqn(3), in units of the string tension, versus $1/N^2$ together with a linear extrapolation in $1/N^2$ to $N = \infty$.

- For the closed flux tube [Athenodorou and Teper(2017)], it is now understood that the worldsheet includes an additional field—the worldsheet axion—which manifests as a massive excitation
  [Dubovsky *et al.*(2013)Dubovsky, Flauger, and Gorbenko, Athenodorou and Teper(2022)].
- Does the same phenomenon occur for the open flux tube?
- Does this state persist in the large-N_c limit?

Why do we need Large N_c?

- At large N_c, the interactions between hadrons are reduced, and we want to test if the world sheet action is preserved.
- What do we expect: we already know that there is a world sheet axion, for closed flux tubes, and that it maintained in the Large N_c limit.
- Previously, we developed pure gauge lattice QCD techniques to study highly excited open flux tubes, with angular momentum Σ, Π, Δ and parities $+$, $-$, g, u.
- For $SU(3)$, we observed in the $-$ parities of the angular momentum Σ, the signal of a world sheet axion.
- Our procedure consists in using our $SU(N_c)$ configuration generator with a CUDA codes for GPUs. We expect to be able to go up, at least, to N_c=6.
- The topological Critical Slowing down may be an obstacle, since in a Monte Carlo sequence the changes in the topological charge Q decrease as an inverse power of N_c.
- Notice a positive point: the finite volume effects decrease at large N_c.

Bosonic String

Excitation	Symmetry	State	
$N = 0$	Σ_g^+	$\|0\rangle$	
$N = 1$	Π_u	$a_{1+}^\dagger \|0\rangle$	$a_{1-}^\dagger \|0\rangle$
$N = 2$	$\Sigma_g^{+\prime}$	$a_{1+}^\dagger a_{1-}^\dagger \|0\rangle$	
	Π_g	$a_{2+}^\dagger \|0\rangle$	$a_{2-}^\dagger \|0\rangle$
	Δ_g	$(a_{1+}^\dagger)^2 \|0\rangle$	$(a_{1-}^\dagger)^2 \|0\rangle$
$N = 3$	$\Sigma_u^{+\prime}$	$(a_{1+}^\dagger a_{2-}^\dagger + a_{1-}^\dagger a_{2+}^\dagger)\|0\rangle$	
	Σ_u^-	$(a_{1+}^\dagger a_{2-}^\dagger - a_{1-}^\dagger a_{2+}^\dagger)\|0\rangle$	
	Π_u'	$a_{3+}^\dagger \|0\rangle$	$a_{3-}^\dagger \|0\rangle$
	Π_u''	$(a_{1+}^\dagger)^2 a_{1-}^\dagger \|0\rangle$	$a_{1+}^\dagger (a_{1-}^\dagger)^2 \|0\rangle$
	Δ_u	$a_{1+}^\dagger a_{2+}^\dagger \|0\rangle$	$a_{1-}^\dagger a_{2-}^\dagger \|0\rangle$
	ϕ_u	$(a_{1+}^\dagger)^3 \|0\rangle$	$(a_{1-}^\dagger)^3 \|0\rangle$

Table 1: Low-lying phonon string states for a fixed ends open string [Juge *et al.*(2003)Juge, Kuti, and Morningstar].

Bosonic String

Excitation	Symmetry	State	
$N = 4$	$\Sigma_g^{+\prime\prime}$	$a_{2+}^\dagger a_{2-}^\dagger \lvert 0\rangle$	
	$\Sigma_g^{+\prime\prime\prime}$	$(a_{1+}^\dagger)^2(a_{1-}^\dagger)^2\lvert 0\rangle$	
	$\Sigma_g^{+(\mathrm{iv})}$	$(a_{1+}^\dagger a_{3-}^\dagger + a_{1-}^\dagger a_{3+}^\dagger)\lvert 0\rangle$	
	Σ_g^-	$(a_{1+}^\dagger a_{3-}^\dagger - a_{1-}^\dagger a_{3+}^\dagger)\lvert 0\rangle$	
	$\Pi_g^\prime$	$a_{4+}^\dagger \lvert 0\rangle$	$a_{4-}^\dagger \lvert 0\rangle$
	$\Pi_g^{\prime\prime}$	$(a_{1+}^\dagger)^2 a_{2-}^\dagger \lvert 0\rangle$	$(a_{1-}^\dagger)^2 a_{2+}^\dagger \lvert 0\rangle$
	$\Pi_g^{\prime\prime\prime}$	$a_{1+}^\dagger a_{1-}^\dagger a_{2+}^\dagger \lvert 0\rangle$	$a_{1+}^\dagger a_{1-}^\dagger a_{2-}^\dagger \lvert 0\rangle$
	$\Delta_g^\prime$	$a_{1+}^\dagger a_{3+}^\dagger \lvert 0\rangle$	$a_{1-}^\dagger a_{3-}^\dagger \lvert 0\rangle$
	$\Delta_g^{\prime\prime}$	$(a_{2+}^\dagger)^2\lvert 0\rangle$	$(a_{2-}^\dagger)^2\lvert 0\rangle$
	$\Delta_g^{\prime\prime\prime}$	$(a_{1+}^\dagger)^3 a_{1-}^\dagger \lvert 0\rangle$	$a_{1+}^\dagger (a_{1-}^\dagger)^3\lvert 0\rangle$
	Φ_g	$(a_{1+}^\dagger)^2 a_{2+}^\dagger \lvert 0\rangle$	$(a_{1-}^\dagger)^2 a_{2-}^\dagger \lvert 0\rangle$
	Γ_g	$(a_{1+}^\dagger)^4\lvert 0\rangle$	$(a_{1-}^\dagger)^4\lvert 0\rangle$

Table 2: Next low-lying phonon string states for a fixed ends open string [Juge *et al.*(2003)Juge, Kuti, and Morningstar].

Bosonic String

- A long flux tube can be understood as a low-energy bosonic string, with the phonon excitations of Tables 1 and 2.
- It describes the dynamics of $D-2$ translational Goldstone bosons.
- These bosons exhibit a non-linearly realized $ISO(1, D-1)$ Poincare symmetry.
- This symmetry is spontaneously broken to the $ISO(1,1) \times O(D-2)$ subgroup.
- As a result, the physics of this string is best described by an action formulated in terms of D worldsheet scalar fields X^{μ}.
- These fields represent the embedding of the string worldsheet into the target spacetime.
- The leading term of this action, in terms of the string tension σ, corresponds to the simplest bosonic string model: the Nambu-Goto action:

$$S = -\sigma \int \mathrm{d}^2 x \sqrt{-\det h_{\alpha\beta}}\,, \tag{1}$$

- The energy spectrum of an open relativistic string with length R and fixed ends is obtained by quantizing Nambu-Goto is given by the Arvis potential [Arvis(1983)]

$$V(R) = \sqrt{\sigma^2 R^2 + 2\pi\sigma\left(N - \frac{(D-2)}{24}\right)}, \tag{2}$$

- where N is the quantum number for string vibrations and D is the dimension of space time. However Nambu-Goto suffers with Weyl anomaly breaking the rotational invariance at $D \neq 26$.

Effective String Theory respecting Lorentz invariance

- Topic received contributions since the early 80s.
  [M. Lüscher '81, J. Polchinski & A. Strominger '90, M. Lüscher & P. Weisz '04, O. Aharony et al '07 – 11, S. Dubovsky et al '12 – 19]
- The expansion in $1/R\sqrt{\sigma}$ yields to:

$$\begin{aligned} E_N(R) &= \sqrt{\sigma}(R\sqrt{\sigma}) \\ &+ \frac{\pi\sqrt{\sigma}}{(R\sqrt{\sigma})}\left(N - \frac{D-2}{24}\right) \\ &- \frac{\pi^2\sqrt{\sigma}}{2(R\sqrt{\sigma})^3}\left(N - \frac{D-2}{24}\right)^2 \\ &+ \frac{\bar{b}_2\pi^3\sqrt{\sigma}}{(R\sqrt{\sigma})^4}\left(B_N^l - \frac{D-2}{60}\right) \\ &+ \frac{\pi^3\sqrt{\sigma}}{16(R\sqrt{\sigma})^5}\left(N - \frac{D-2}{24}\right)^3 + \frac{\pi^3\sqrt{\sigma}(D-26)}{48(R\sqrt{\sigma})^5}C_N^l + \left(\frac{1}{(R\sqrt{\sigma})^6}\right) \end{aligned}$$

- B_N^l and C_N^l are due to the boundaries of the open string.
- This relates to Nambu-Goto via:

$$E_N(R) = E_{\mathrm{NG}}(N,R) + \frac{\bar{b}_2\pi^3\sqrt{\sigma}}{(R\sqrt{\sigma})^4}\left(B_N^l - \frac{D-2}{60}\right) + \frac{\pi^3\sqrt{\sigma}(D-26)}{48(R\sqrt{\sigma})^5}C_N^l + \left(\frac{1}{(R\sqrt{\sigma})^6}\right)$$

The Axionic String Ansatz (ASA)

- Lattice calculations demonstrate that there is one massive resonance in the closed flux tube [Athenodorou *et al.*(2011a)Athenodorou, Bringoltz, and Teper, Athenodorou *et al.*(2011b)Athenodorou, Bringoltz, and Teper, Athenodorou and Teper(2019), Athenodorou *et al.*(2023)Athenodorou, Dubovsky, Luo, and Teper].
- One can add a massive resonance [Dubovsky *et al.*(2013)Dubovsky, Flauger, and Gorbenko, Dubovsky *et al.*(2015)Dubovsky, Flauger, and Gorbenko],

$$S_\phi = \int d^2\sigma \sqrt{-h} \left(-\frac{1}{2}(\partial\phi)^2 - \frac{1}{2}m^2\phi^2 + \frac{Q_\phi}{4} h^{\alpha\beta} \epsilon_{\mu\nu\lambda\rho} \partial_\alpha t^{\mu\nu} \partial_\beta t^{\lambda\rho} \phi \right) , \qquad (3)$$

- ϕ is a pseudoscalar – the world-sheet axion.
- From Monte-Carlo data of Yang-Mills: $Q_\phi \sim 0.38 \pm 0.04$, $m_\phi \sqrt{\sigma} \sim 1.85$ in $SU(3)$
- IWith the value $Q_{\rm int} = \sqrt{7/(16\pi)}$, the theory is fully integrable at leading order.

Our lattice framework to study the flux tube

- In this work, we focus on the large-distance behavior of the excited spectrum, deliberately avoiding short-distance effects. To achieve this, we employ the Wilson action discretized on anisotropic lattices [Morningstar(1997), Bicudo *et al.*(2021)Bicudo, Cardoso, and Sharifian], which is expressed as:

$$S_{\text{Wilson}} = \beta \left(\frac{1}{\xi} \sum_{x,s>s'} P_{s,s'} + \xi \sum_{x,s} P_{s,t} \right), \tag{4}$$

  $P_{s,s'}$ represents the spatial plaquettes, and $P_{s,t}$ the spatial-temporal plaquettes.

- $\beta = 6/g^2$ is the inverse coupling constant and ξ represents the bare anisotropy factor, defined as the ratio of the spatial to temporal lattice spacings (a_s/a_t).
- The renormalized anisotropy factor will be denoted ξ'.
- By using an anisotropic action, we achieve finer lattice spacing in the temporal direction and a coarser spacing in the spatial direction.
- This results in more data points for the effective mass plot, ideal for the study of excited states.
- This also enables the study of larger distances. The ensembles generated with this action are listed in Table 3.
- We generate the $SU(N_c)$ configurations with revising the CUDA codes for GPUs of Ref. [Cardoso and Bicudo(2013)].

Our lattice framework to study the flux tube

Ensemble	N_c	β	ξ	ξ_r	Volume	$a_t\sqrt{\sigma}$	$a_s\sqrt{\sigma}$
$W_{3,2}$	3	5.90	2.00	2.1737(4)	$24^3 \times 48$	0.1403(8)	0.3049(17)
$W_{3,4}$	3	5.70	4.00	4.5363(8)	$24^3 \times 96$	0.0887(4)	0.4023(16)
$W_{4,2}$	4	10.70	2.00	2.0958(2)	$24^3 \times 48$	0.1680(2)	0.3521(5)
$W_{4,4}$	4	10.40	4.00	4.2940(5)	$24^3 \times 96$	0.1018(3)	0.4372(12)
$W_{5,2}$	5	17.20	2.00	2.0596(1)	$24^3 \times 48$	0.1451(3)	0.2988(5)
$W_{5,4}$	5	16.50	4.00	4.1853(3)	$24^3 \times 96$	0.1025(0)	0.4288(1)
$W_{6,4}$	6	24.00	4.00	4.1274(2)	$24^3 \times 96$	0.0996(0)	0.4113(2)

Table 3: Details for the ensembles generated using the anisotropic Wilson action. ξ_r is the normalized anisotropic factor, and each ensemble includes 1000 configurations. All ensembles have been smeared 100 times using multihit in the temporal direction and APE smearing ($\alpha = 0.3$, $n_s = 20$) in the spatial directions.

Topological Charge

- The topological charge is defined with the field strength tensor of the gauge field,

$$Q = \frac{1}{32\pi^2} \int d^4x \, \epsilon_{\mu\nu\rho\sigma} \mathrm{Tr}\left[G_{\mu\nu}(x) G_{\rho\sigma}(x)\right] \, . \tag{5}$$

- As N_c increases, the topological charge tends to freeze.
- It is crucial to track the topological charge to ensure the ergodicity of the Monte Carlo process.

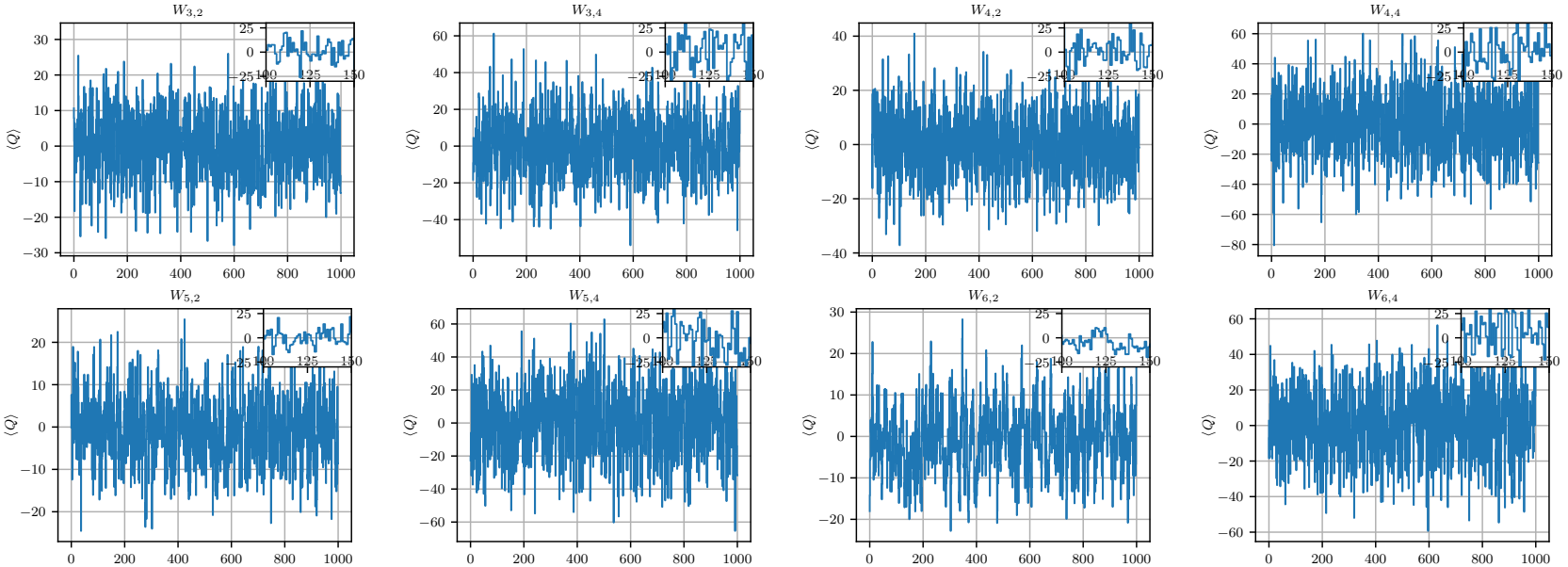

Figure 2: Topological charge history for $SU(3)$, $SU(4)$, $SU(5)$ and $SU(6)$ and anisotropy 2 and 4. In our simulation, the topological charge is not frozen, and thus the simulation is ergodic.

Generalized Eigenvalue Problem

- To compute the spectra of the flux tube, we first calculate the Wilson correlation matrix $\mathcal{C}(r, t)$.
- The entry $\mathcal{C}_{i,j}(r, t)$ of the Wilson correlation matrix is the expectation value of spatial-temporal closed loops (Fig. 4), where the symmetry is provided by the spatial operators O_i and O_j.
- For example, O_i and O_j can be constructed using the staples shown in Figs. 5, 7, 6, 8.
- Next, we find the generalized eigenvalues λ of the Wilson correlation matrix:

$$\mathcal{C}(r, t)\vec{v}_n = \lambda_n(r, t)\mathcal{C}(r, t_0)\vec{v}_n, \tag{6}$$

  where we set $t_0 = 0$, and obtain a set of time-dependent eigenvalues $\lambda_n(t)$ for each r.
- We then order the eigenvalues and plot the effective mass defined as:

$$E_i(r) = \ln \frac{\lambda_i(r, t)}{\lambda_i(r, t + 1)}. \tag{7}$$

  The value of the plateau in the effective mass plot yields the energy $E_i(r)$ of the flux tube.

The quantum numbers of the flux tube

There are three constants of motion whose eigenvalues are used to label the quantum state of the flux tube:

- z-component of angular momentum $\Lambda = 0, 1, 2, 3, \ldots$, they are typically denoted by greek letters $\Sigma,\ \Pi,\ \Delta,\ \Phi, \ldots$, respectively
- Combination of the charge conjugation and spatial inversion with respect to the mid point of the charge axis operators $\mathcal{P}o\mathcal{C}$, its eigenvalues $\eta = 1, -1$, they are denoted by $g,\ u$, respectively.
- For $\Sigma(\Lambda = 0)$, reflection with respect to a plan containing the charge axis, $\mathcal{P}_x$, with eigenvalues $\epsilon = +, -$.

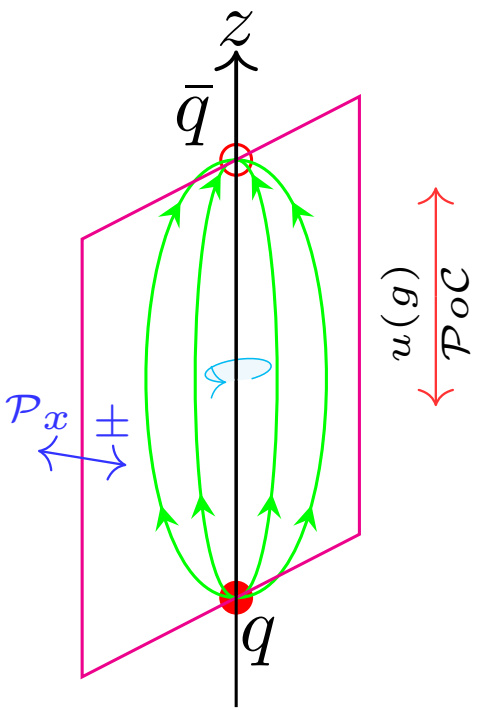

Figure 3: The possible quantum numbers are: $\Sigma_g^+, \Sigma_g^-, \Sigma_u^+, \Sigma_u^-, \Pi_g, \Pi_u, \Delta_u, \Delta_g, \ldots$

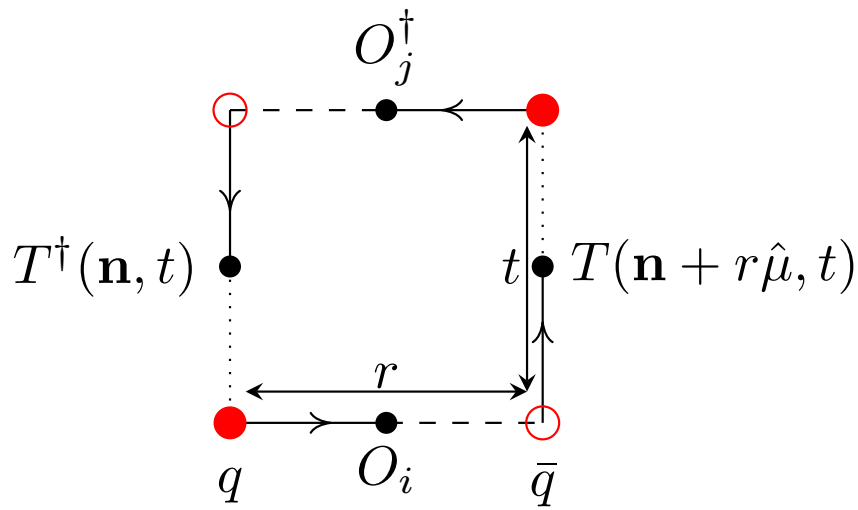

Figure 4: A closed loop corresponds to the entry $\mathcal{C}_{i,j}(r, t)$ of the Wilson correlation matrix.

Operators with the flux tube quantum numbers

- We use the operators, shown in Figs 5, 7, 6, 8, of Ref. [Sharifian *et al.*(2023)Sharifian, Cardoso, and Bicudo] to study $SU(3)$ spectra.

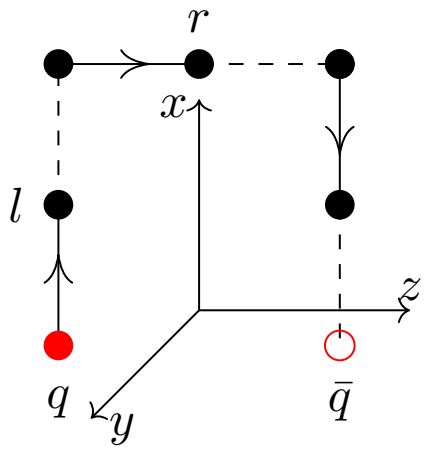

Figure 5: Staples for Σ_g^+, Π_u, and Δ_g flux tubes.

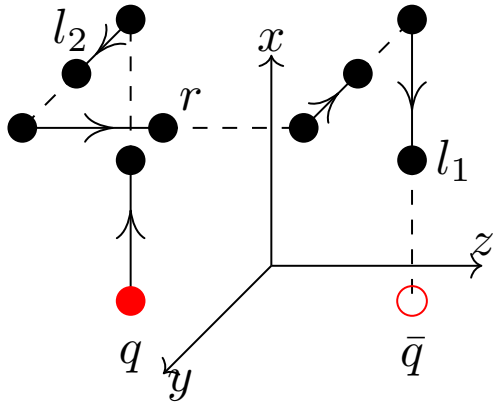

Figure 6: Staples for Σ_g^- flux tubes.

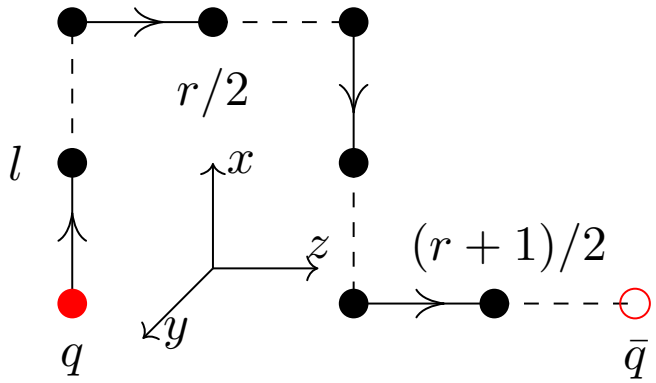

Figure 7: Staples for Σ_u^+,$O^{\Pi g}$,and $O^{\Delta u}$ flux tubes.

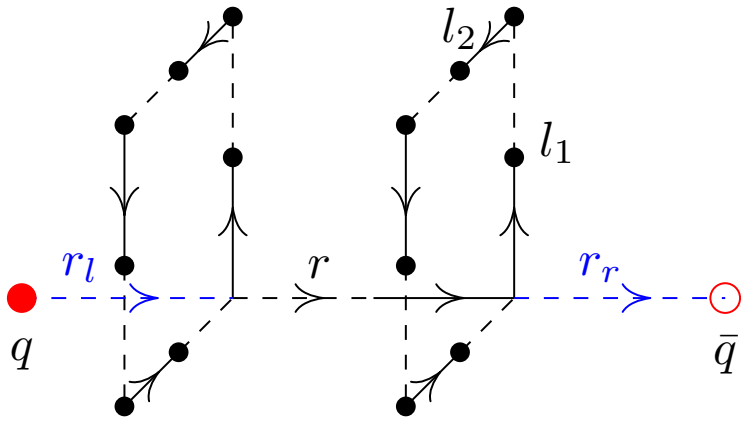

Figure 8: Staples for Σ_u^- flux tubes.

Results on the spectrum of the open flux-tube

- In this section, we present our findings on the spectra for $N_c = 3, 4, 5$ and $N_c = 6$, across the eight irreducible representations: Σ_g^+, Σ_g^-, Σ_u^+, Σ_u^-, Π_g, Π_u, Δ_g, and Δ_u.
- We present results at two different lattice spacings and anisotropies to examine whether the spectrum's behavior changes as we approach the continuum limit.
- The focus of this work is on comparing the spectra with the Nambu-Goto string to investigate potential axion signatures.
- The absolute ground state corresponds to the Σ_g^+ representation, closely approximated by the Arvis potential except for small $1/R(\sqrt{\sigma})^4$ deviations [Aharony and Karzbrun(2009)].
- This ground state can be interpreted as the vacuum state $|0\rangle$, with no phonon operators acting on it, implying that no scattering processes occur along the string's worldsheet.
- The first excited state is the ground state of Π_u, it also agrees to a quite good accuracy with the Nambu-Goto state $\alpha_\pm^\dagger|0\rangle$ [Sharifian *et al.*(2023)Sharifian, Cardoso, and Bicudo].
- Then we study the highest possible excitations observable in our framework.

Results on the spectrum of the open flux-tube

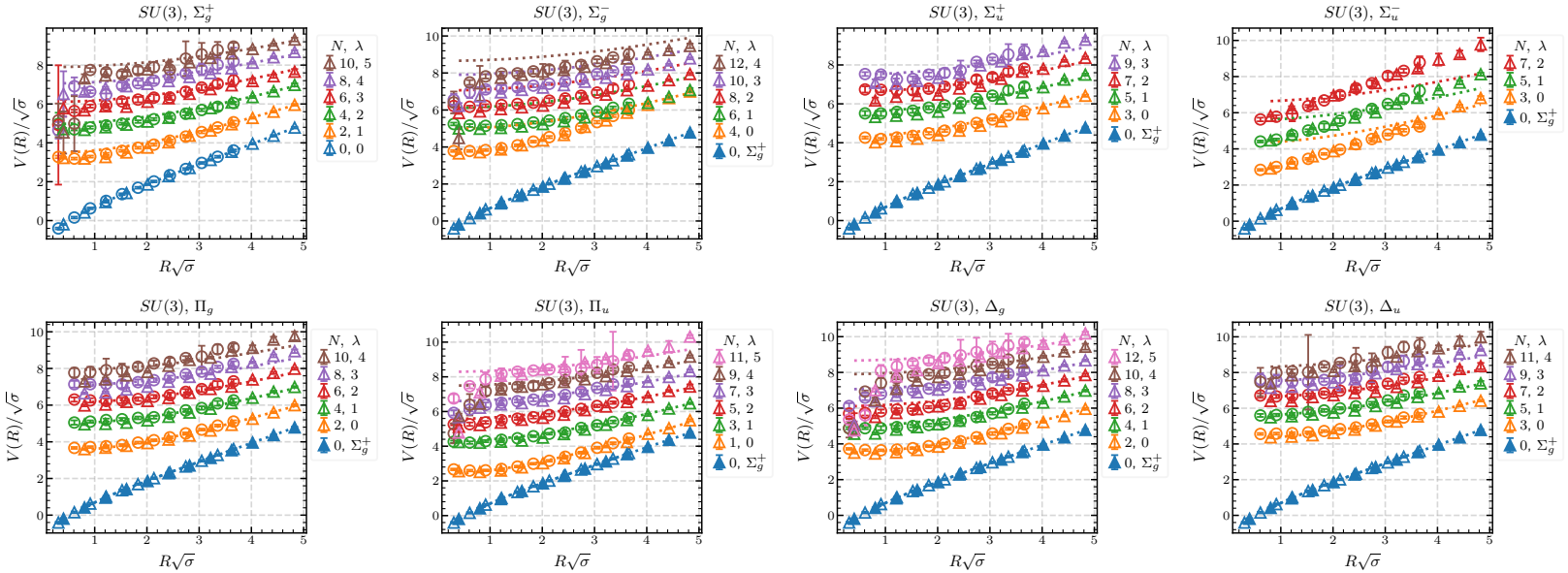

Figure 9: Eight SU(3) spectra. Polygonal shapes in each figure show the simulation with $\xi = 4$, while circle markers indicate $\xi = 2$. N is the quantum number as defined in Eq. 2, and λ is the excitation number.

Results on the spectrum of the open flux-tube

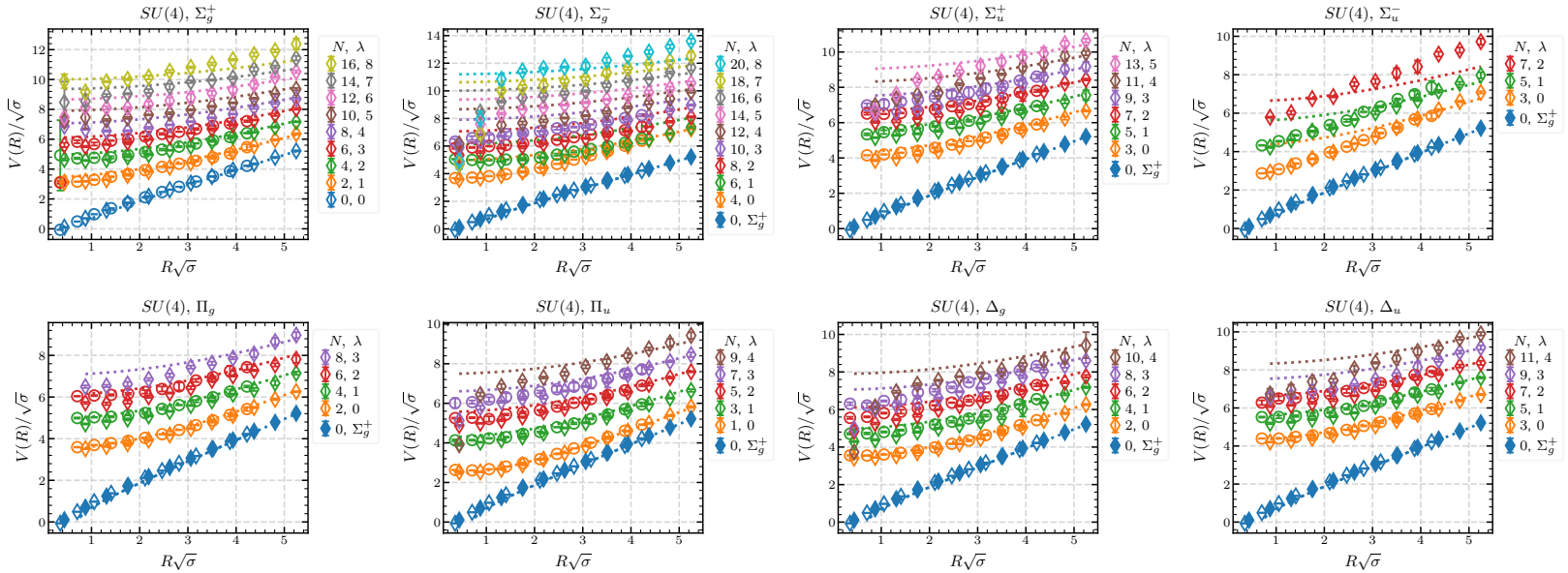

Figure 10: Eight SU(4) spectra. Polygonal shapes in each figure show the simulation with $\xi = 4$, while circle markers indicate $\xi = 2$. N is the quantum number as defined in Eq. 2, and λ is the excitation number.

Results on the spectrum of the open flux-tube

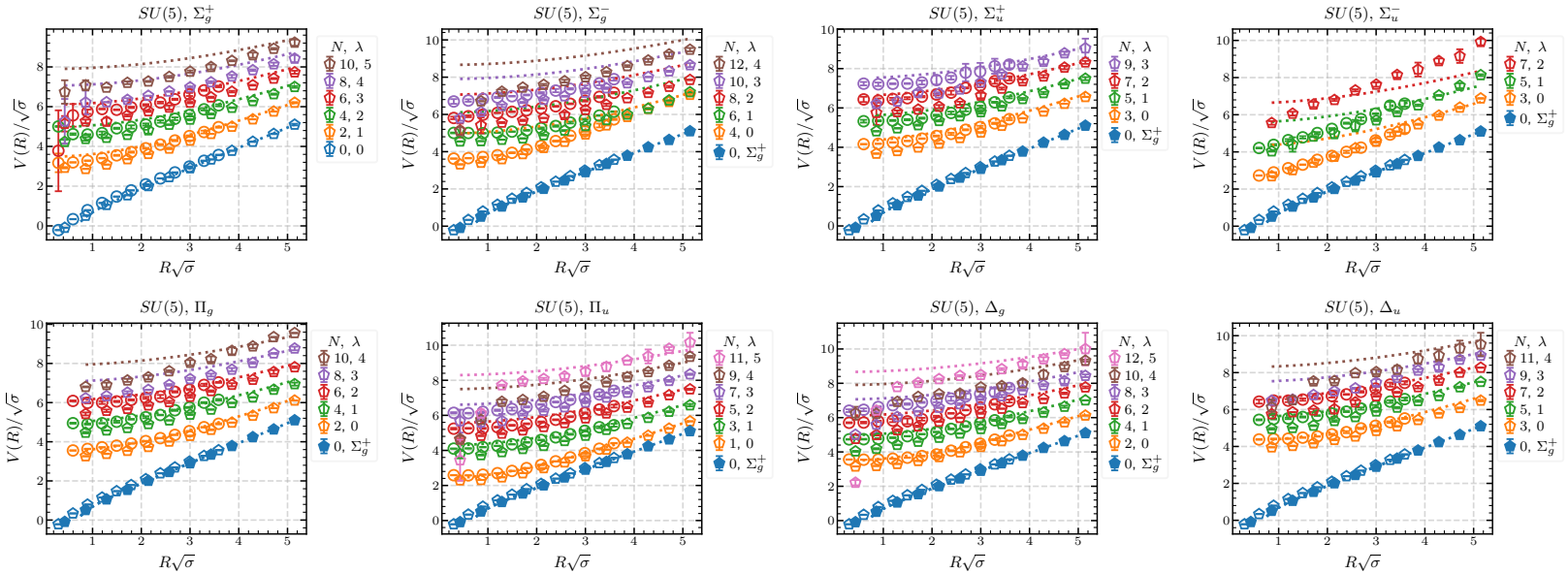

Figure 11: Eight SU(5) spectra. Polygonal shapes in each figure show the simulation with $\xi = 4$, while circle markers indicate $\xi = 2$. N is the quantum number as defined in Eq. 2, and λ is the excitation number.

Results on the spectrum of the open flux-tube

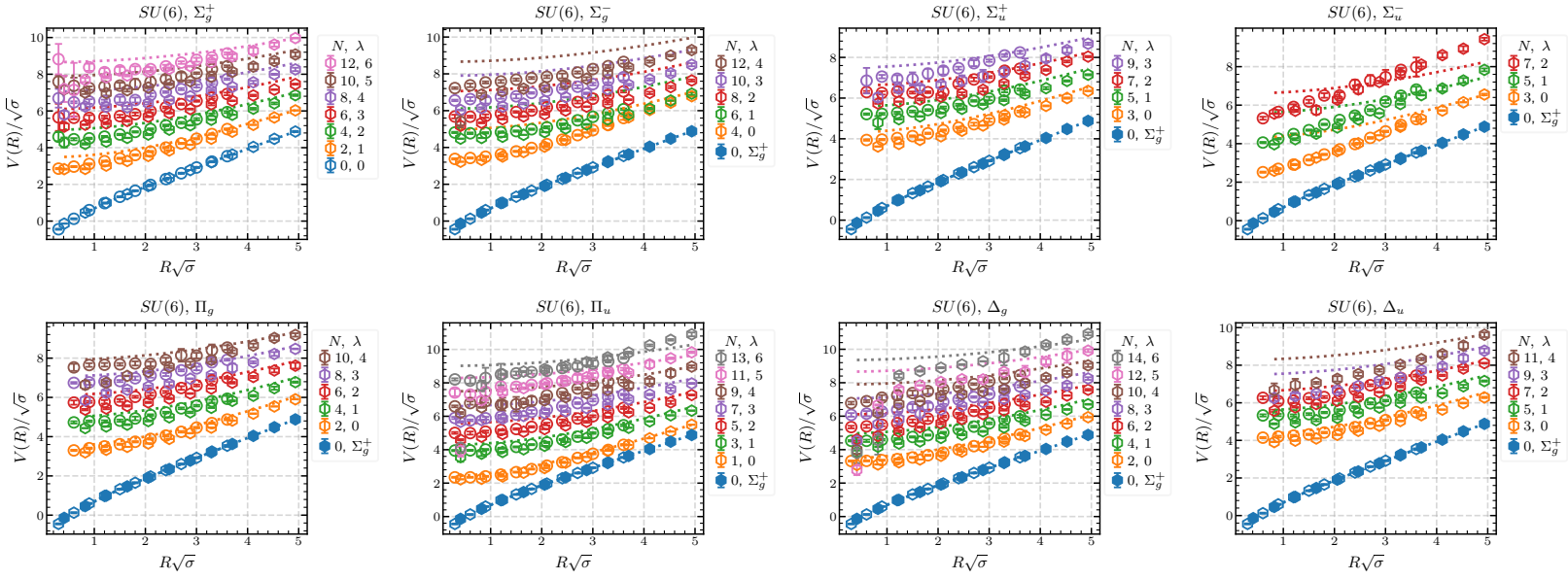

Figure 12: Eight SU(6) spectra. Polygonal shapes in each figure show the simulation with $\xi = 4$, while circle markers indicate $\xi = 2$. N is the quantum number as defined in Eq. 2, and λ is the excitation number.

Axion masses

- As we examine higher excited states, we observe some significant deviations from Nambu-Goto behavior, in the ground state of Σ_g^- and across the entire spectrum of Σ_u^-.
- Considering the spectra shown in Figs. 9, 10, 11 and 12, we observe that the Σ_u^- flux tube and the ground state of Σ_g^- are not compatible with the Nambu-Goto model.

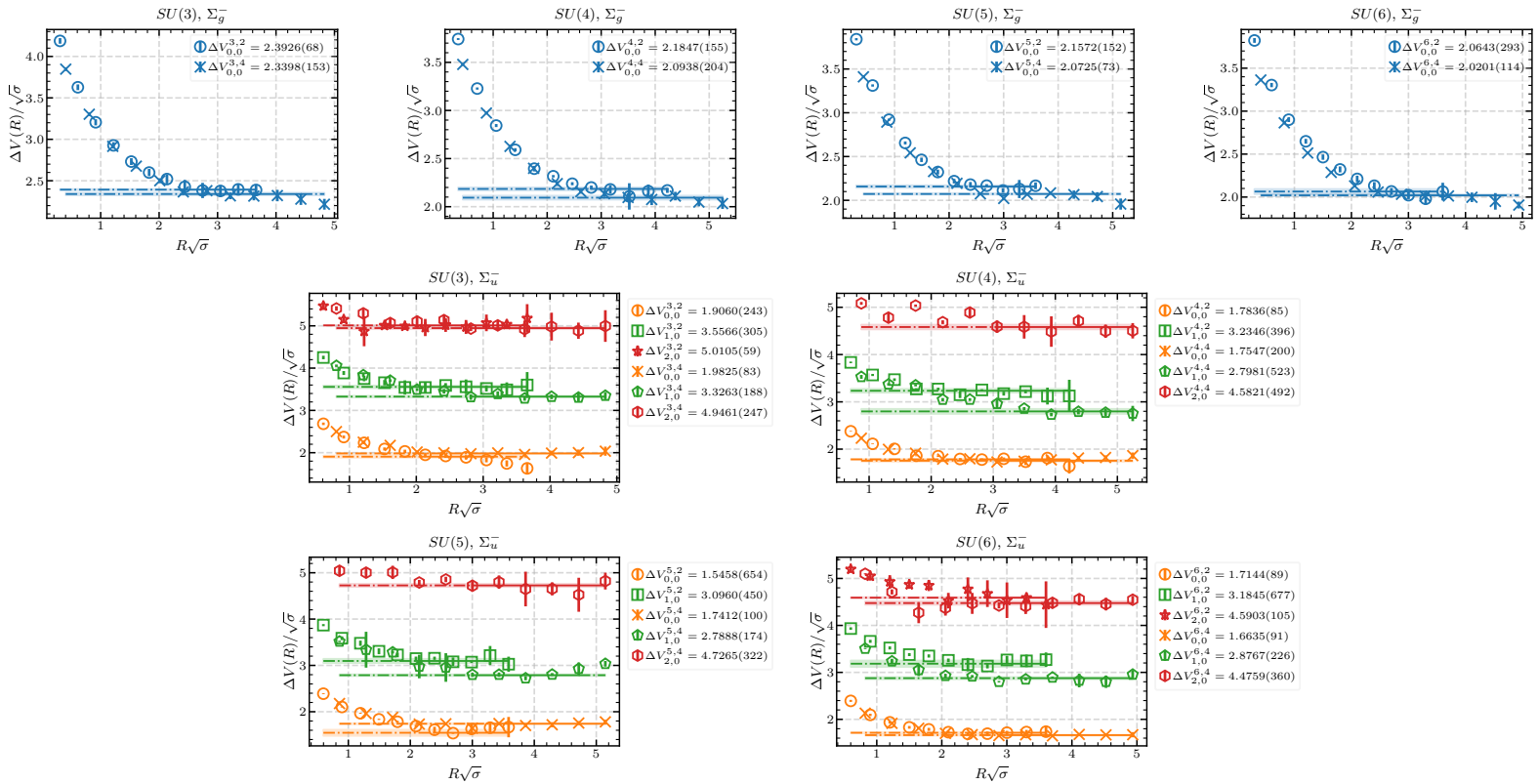

Figure 13: We subtract the groundstate potential to find evidence for axions, for different groups. $\Delta V_{p,0}^{m,n}$ indicates the data from ensemble $W_{m,n}$ in Table 3, and $V_{\Sigma_u^- p} - V_{\Sigma_g^+}$ where p is the excitation number.

Axion masses

- These states exhibit behavior akin to that of a ground state with an additional constant mass term coupled, as illustrated in Figs. 9, 10, 11 and 12.
- This behavior aligns with expectations for an axion coupled to the string. In Figs. 13 and 14, the lightest axion mass is identical to the one observed in the closed flux tube spectra.

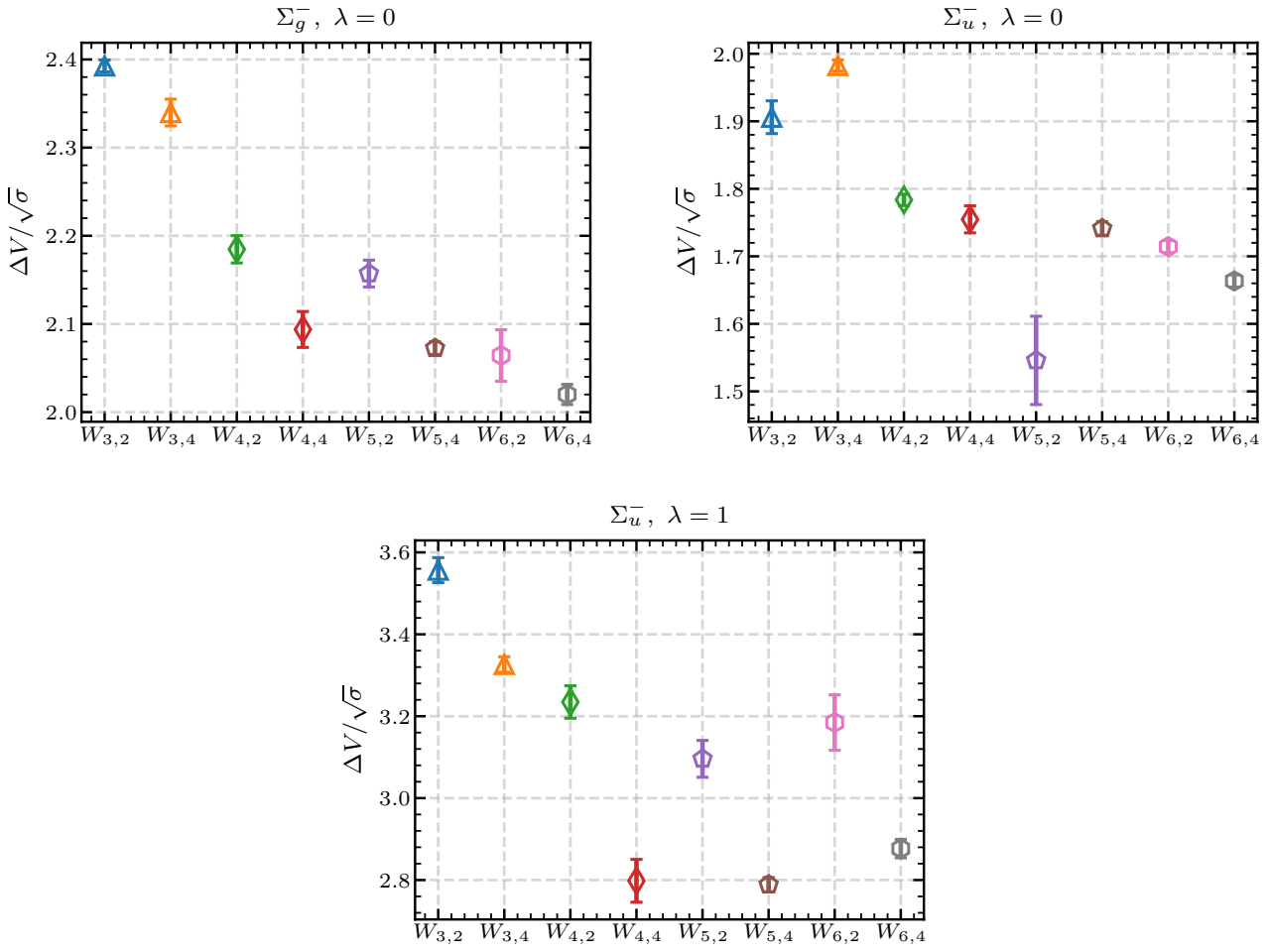

Figure 14: We compare the axion masses as a function of N_c.

Conclusion

In this study, we conducted a comprehensive analysis of the spectrum of the open flux tube.

- Specifically, we extracted the spectrum for $SU(3)$, $SU(4)$, $SU(5)$ and $SU(6)$ gauge theories, each one at two different anisotropies and lattice spacings.
- Moreover we measured the history of the topological charge for anisotropic lattices and find that up to Nc=6 our simulations are ergodic.
- Our findings reveal that most of the states in the spectra of the flux tube at large source distances can be well approximated by the Nambu-Goto string model.
- However, several states exhibit significant deviations from the Nambu-Goto string behavior, displaying characteristics of massive excitations.
- Notably, the lightest of these massive "axions" has a mass matching its counterpart found in the closed flux tube.
- Several possible continuations of the present work are in view, such as
  - a more detailed study of the flux tube at shorter distances,
  - a better characterization of the axions with a wider basis of operators,
  - a calibration of the topological effects,
  - finite temperature exploration.

Acknowledgment

AS was supported by CEFEMA UIDB/04540/2020 Post-Doctoral Research Fellowship. AA acknowledges support by the “EuroCC" project funded by the “Deputy Ministry of Research, Innovation and Digital Policy and the Cyprus Research and Innovation Foundation" as well as by the European High-Performance Computing Joint Undertaking (JU) under grant agreement No 101101903. The authors thank CeFEMA, an IST research unit whose activities are partially funded by FCT contract UIDB/04540 for R&D Units.

References I


A. Sharifian, N. Cardoso, and P. Bicudo, Physical Review D **107**, 10.1103/physrevd.107.114507 (2023).


A. Athenodorou and M. Teper, Phys. Lett. B **771**, 408 (2017), arXiv:1702.03717 [hep-lat] .


S. Dubovsky, R. Flauger, and V. Gorbenko, Phys. Rev. Lett. **111**, 062006 (2013), arXiv:1301.2325 [hep-th] .


A. Athenodorou and M. Teper, PoS **LATTICE2021**, 103 (2022), arXiv:2112.11213 [hep-lat] .


K. J. Juge, J. Kuti, and C. Morningstar, in *International Conference on Color Confinement and Hadrons in Quantum Chromodynamics - Confinement 2003* (2003) pp. 221–232, arXiv:hep-lat/0312019 .


J. Arvis, Physics Letters B **127**, 106 (1983).


A. Athenodorou, B. Bringoltz, and M. Teper, JHEP **02**, 030, arXiv:1007.4720 [hep-lat] .


A. Athenodorou, B. Bringoltz, and M. Teper, JHEP **05**, 042, arXiv:1103.5854 [hep-lat] .


A. Athenodorou and M. Teper, JHEP **01**, 063, arXiv:1811.06280 [hep-lat] .


A. Athenodorou, S. Dubovsky, C. Luo, and M. Teper, JHEP **05**, 082, arXiv:2301.00034 [hep-lat] .


S. Dubovsky, R. Flauger, and V. Gorbenko, J. Exp. Theor. Phys. **120**, 399 (2015), arXiv:1404.0037 [hep-th] .

References II


C. Morningstar, Nuclear Physics B - Proceedings Supplements **53**, 914 (1997).


P. Bicudo, N. Cardoso, and A. Sharifian, Phys. Rev. D **104**, 054512 (2021), arXiv:2105.12159 [hep-lat] .


N. Cardoso and P. Bicudo, Comput. Phys. Commun. **184**, 509 (2013), arXiv:1112.4533 [hep-lat] .


O. Aharony and E. Karzbrun, JHEP **06**, 012, arXiv:0903.1927 [hep-th] .